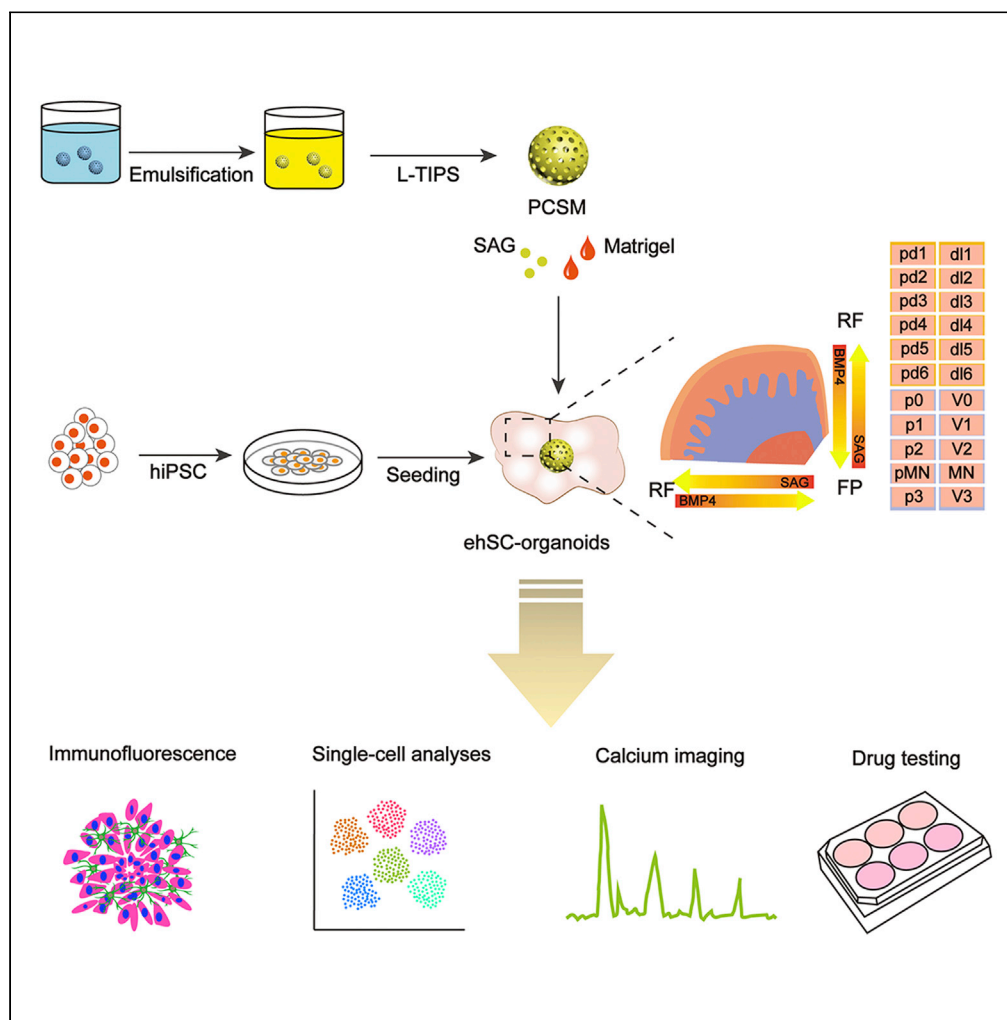


Article

# Generation of dorsoventral human spinal cord organoids via functionalizing composite scaffold for drug testing



Weiwei Xue, Bo Li, Huihui Liu, ..., Lei Ren, Huijuan Li, Zhicheng Shao

www.xue@fudan.edu.cn (W.X.)  
zcsiao@fudan.edu.cn (Z.S.)

Highlights

PCSM-Matrigel@SAG is useful for induction of human dorsoventral spinal cord organoids

The ehSC-organoids contain human spinal cord-like dorsoventral cytoarchitecture

The ehSC-organoids could be used to mimic motor neuron diseases for drug testing



## Article

## Generation of dorsoventral human spinal cord organoids via functionalizing composite scaffold for drug testing

Weiwei Xue,<sup>1,4,\*</sup> Bo Li,<sup>1,2,4</sup> Huihui Liu,<sup>1,4</sup> Yujie Xiao,<sup>3</sup> Bo Li,<sup>3</sup> Lei Ren,<sup>2</sup> Huijuan Li,<sup>1</sup> and Zhicheng Shao<sup>1,5,\*</sup>

## SUMMARY

The spinal cord possesses highly complex, finely organized cytoarchitecture guided by two dorsoventral morphogenic organizing centers. Thus, generation of human spinal cord tissue *in vitro* is challenging. Here, we demonstrated a novel method for generation of human dorsoventral spinal cord organoids using composite scaffolds. Specifically, the spinal cord ventralizing signaling Shh agonist (SAG) was loaded into a porous chitosan microsphere (PCSM), then thermosensitive Matrigel was coated on the surface to form composite microspheres with functional sustained-release SAG, termed as PCSM-Matrigel@SAG. Using PCSM-Matrigel@SAG as the core to induce 3D engineering of human spinal cord organoids from human pluripotent stem cells (ehSC-organoids), we found ehSC-organoids could form dorsoventral spinal cord-like cytoarchitecture with major domain-specific progenitors and neurons. Besides, these ehSC-organoids also showed functional calcium activity. In summary, these ehSC-organoids are of great significance for modeling spinal cord development, drug screening as 3D models for motor neuron diseases, and spinal cord injury repair.

## INTRODUCTION

The spinal cord tissue is vital for sensory and motor functional regulation of human body. The damage or degeneration of the spinal cord and its well-organized cytoarchitecture, such as in spinal cord injury (SCI) or motor neuron diseases (MNDs),<sup>1,2</sup> leads to motor dysfunction, increasing social burden and impairing quality of life.<sup>3</sup> Currently, available animal or *in vitro* two-dimensional (2D) models often do not accurately reflect pathology of human spinal cord diseases, hampering mechanistic studies and development of new therapies. Thus, it is urgent to develop a three-dimensional (3D) model of the human spinal cord for further studies of the mechanisms of MNDs, screening drugs, and developing SCI therapies.

During spinal cord development, the territory of spinal cord progenitor cells is guided by two organizing centers.<sup>4–8</sup> One, the roof plate (RP), is located on the dorsal side and induces the dorsal domains of progenitor cells by producing dose gradient of bone morphogenetic proteins (BMPs) and wingless ints (WNTs). The other, the floor plate (FP), is located on the ventral side and induces the ventral progenitor domains by releasing sonic hedgehog (Shh). With the induction of these two morphogenetic organizing centers, 6 discrete dorsal progenitor domains and 5 ventral progenitor domains are patterned along the dorsal-ventral axis, and various spinal cord subtype neurons including motor neurons were generated from specific ventral progenitor domains.<sup>9–12</sup> Previous methods of inducing spinal cord organoids have been reported.<sup>13,14</sup> Recent studies have shown that the long-range functional connections within these organoids could resemble those in cerebral cortical spheroids and hindbrain/cervical spinal cord spheroids, which were integrated by modular assembloid approaches.<sup>15,16</sup> Our recent study reported that human astrocytes can be directly reprogrammed into early neuroectodermal cells, paving the way for generation of spinal cord organoids used for SCI repair.<sup>17</sup> However, organoids generated from these methods could not completely establish spatial dorsoventral cytoarchitecture like the human spinal cord. Furthermore, with increasing size, the center of 3D spinal cord organoid showed necrosis due to a lack of nutrients, which limits applications in modeling spinal cord development and MNDs or studying regeneration of SCI and drug screening.

Biomaterials play important roles in tissue engineering and repair.<sup>18</sup> In recent years, porous chitosan microspheres (PCSMs), with excellent sphere-forming ability and biocompatibility, have been widely applied in

<sup>1</sup>Institute for Translational Brain Research, State Key Laboratory of Medical Neurobiology, MOE Frontiers Center for Brain Science, Institute of Pediatrics, National Children's Medical Center, Children's Hospital, Fudan University, Shanghai 200032, China

<sup>2</sup>Key Laboratory of Biomedical Engineering of Fujian Province University/Research Center of Biomedical Engineering of Xiamen, Department of Biomaterials, College of Materials, Xiamen University, Xiamen 361005, China

<sup>3</sup>Department of Neurosurgery, Huashan Hospital, Institute for Translational Brain Research, State Key Laboratory of Medical Neurobiology, MOE Frontiers Center for Brain Science, Fudan University, Shanghai 200032, China

<sup>4</sup>These authors contributed equally

<sup>5</sup>Lead contact

\*Correspondence: [wxue@fudan.edu.cn](mailto:wxue@fudan.edu.cn) (W.X.), [zcshao@fudan.edu.cn](mailto:zcshao@fudan.edu.cn) (Z.S.)  
<https://doi.org/10.1016/j.isci.2022.105898>



cell culture and drug delivery systems because they can be degraded into nontoxic products *in vivo*.<sup>19,20</sup> Temperature-sensitive Matrigel is a matrix material containing growth factors for supporting human pluripotent stem cell growth and cell adherence. Thus, we hypothesized that the combination of PCSM and Matrigel with loading Shh agonist (SAG), a Shh signaling activator, (termed PCSM-Matrigel@SAG) could form a functional composite scaffold. This scaffold would mimic the ventral spinal cord organizing centers, releasing SAG for the spatial specification of human spinal cord organoids.

Here, we successfully established an innovative method to generate engineered human spinal cord organoids (ehSC-organoids) via PCSM-Matrigel@SAG composite scaffolds *in vitro*. These ehSC-organoids demonstrate distinct human ventral and dorsal spinal cord progenitor domains and major subtype neurons via immunostaining and single-cell RNA sequencing. Importantly, these ehSC-organoids showed neuronal calcium activity and can be utilized in drug screening as 3D models.

## RESULTS

### Preparation and characterization of PCSM-Matrigel@SAG composite materials

In order to prepare a composite scaffold with sustained release of the ventral signaling compound SAG, a combination of microemulsification and low-temperature thermally induced phase separation techniques was used to prepare PCSM, then small-molecule SAG was loaded into the PCSM through gelation using thermosensitive Matrigel (Figure 1A). The PCSMs showed classical microspheres with a uniform size ranging from 400 to 600  $\mu\text{m}$  (Figures 1B and 1C). The micropores, around 15 to 25  $\mu\text{m}$  in diameter, were revealed to be uniformly distributed in PCSMs using scanning electron microscopy (SEM) (Figures 1D and S1B). Furthermore, a nitrogen-adsorption assay was used to confirm the pore size of the PCSM. Results showed that the pore size of the PCSM was on average  $15 \pm 5 \mu\text{m}$  (Figures 1D and 1G), which was consistent with the pore size measured by SEM. After coating with Matrigel, we found that the size of PCSMs was not obviously changed, but the surface became smoother, and the micropores were fully filled by Matrigel (Figures 1E and 1F). In order to verify the sustained-release function of these composite materials, the PCSM was loaded with 0.1-mM SAG and coated with a high concentration of Matrigel to combine as functional composite scaffolds, termed PCSM-Matrigel@SAG. To test the release of small-molecule SAG, PCSM-Matrigel@SAG was dipped in PBS to mimic cell culture conditions, and the phosphate buffered saline (PBS) solution was collected every two days. After 18 days, the concentration of SAG in the PBS solution was measured by UV spectrophotometer according to the absorption spectrum of the standard SAG solution (Figure S1A). The results showed that the release of SAG gradually increased from day 0 to day 10, reaching the maximum concentration at day 10, indicating PCSM-Matrigel@SAG could sustain long-term release of SAG (Figure 1H). Finally, we tested the toxicity of PCSMs by 3-(4,5-dimethyl-2-thiazolyl)-2,5-diphenyl-2-H-tetrazolium bromide, Thiazolyl Blue Tetrazolium Bromide (MTT) assay. The results showed that PCSMs demonstrate safety and nontoxicity in human embryonic stem cells (hESCs) (Figure 1I). Taken together, these data show PCSM-Matrigel@SAG are safe composite scaffolds which can be used for the sustained release of small molecules.

### PCSM-Matrigel@SAG scaffolds mimic the ventral spinal cord organizer for the induction of ehSC-organoids

Next, PCSM-Matrigel@SAG scaffolds were used to construct spinal cord topography-like tissue. We conducted the induction of developmental spinal cord organoids from human hESCs *in vitro* (Figure 2A). We further improved the method of differentiation of the spinal cord organoids according to the previous studies (Figure 2B).<sup>13</sup> After 3-day induction, we observed that hESCs were well integrated with PCSM-Matrigel@SAG (Figure 2C). However, the cells did not aggregate with PCSMs that were not coated with Matrigel (Figure S2A). This result indicates that Matrigel facilitated the attachment of hESCs. After 14 days, ehSC-organoids grown using PCSM-Matrigel@SAG scaffolds grew well and developed a small number of neuroepithelial-like buds (Figure 2C). After coating with Matrigel, the growth rate of ehSC-organoids was accelerated, and ehSC-organoids showed neuron migration and neurite growth (Figures 2C and 2D). At day 21, the size of ehSC-organoids grew to a maximum of 3 mm, larger than those grown without PCSM-Matrigel@SAG (Figures 2D and S2B). In order to verify the spinal cord domain-specific progenitors of the ehSC-organoids, these organoids were subsequently sectioned, and immunostaining was performed. The results showed that many ventral NKX6.1+ progenitor cells were adjacent to the PCSM-Matrigel@SAG organizer, which released ventral signaling SAG, in relevant organoids, but were randomly distributed in organoids without the PCSM-Matrigel@SAG organizer (Figures 2E and 2F). Some cells were also colabeled with MAP2, indicating their neuronal identity (Figure 2G). Specific ventral motor neuron

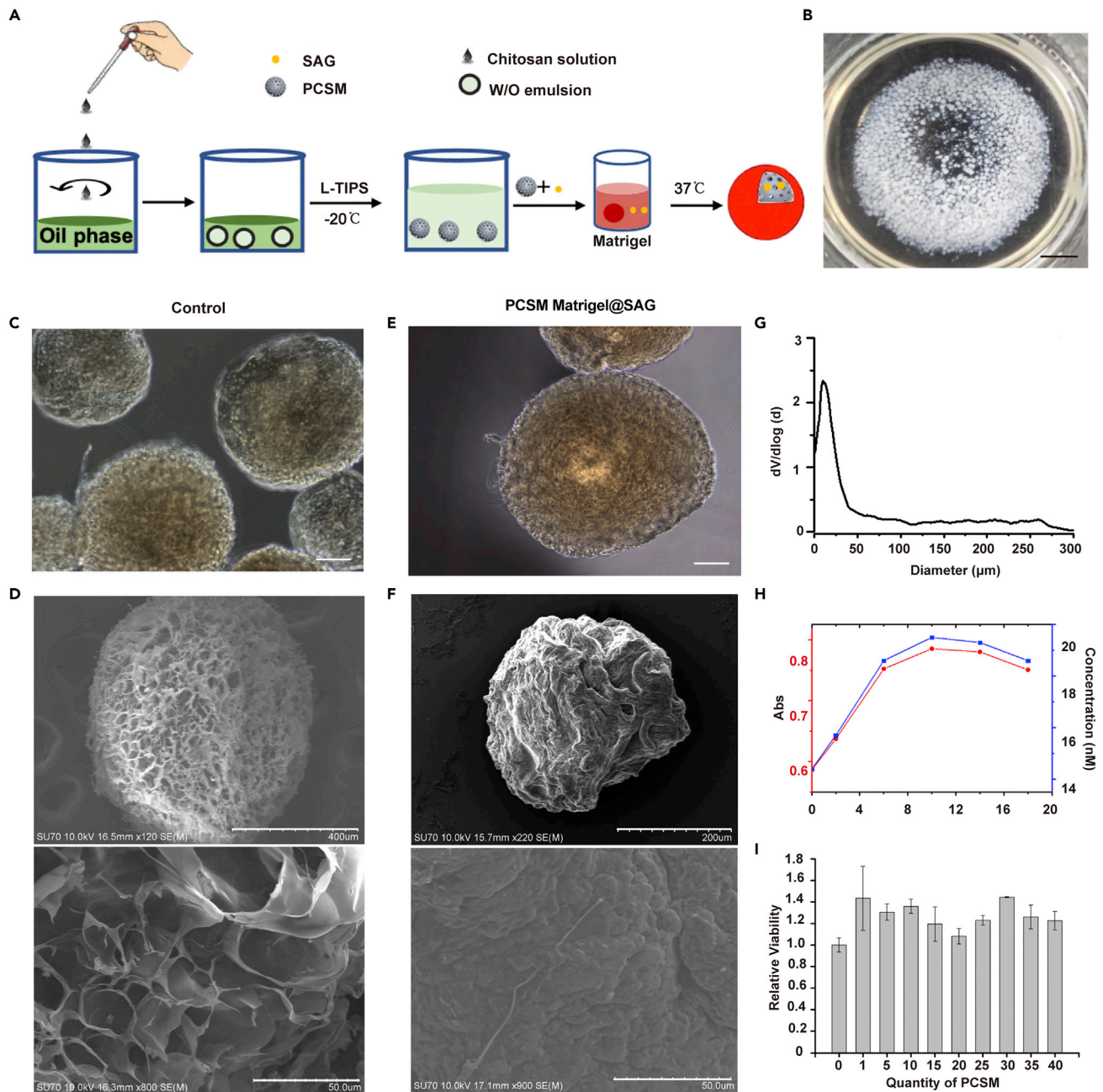


**Figure 1. Preparation and characterization of PCSM-Matrigel@SAG**

(A) Schematic diagram of PCSM preparation.

(B) Bulk of PCSM. Scale bars, 5 mm.

(C) Image of PCSM. Scale bars, 200 μm.

(D) SEM image of PCSM. Scale bars: 400 μm (up) and 50 μm (down).

(E) Image of PCSM coated with Matrigel. Scale bars, 200 μm.

(F) SEM image of PCSM coated with Matrigel. Scale bars: 200 μm (up) and 50 μm (down).

(G) Pore size distribution of PCSM.

(H) Concentration curve of the Matrigel-coated microspheres releasing SAG from day 0 to 18 as measured by UV spectrophotometer.

(I) Toxicity assay of PCSM.

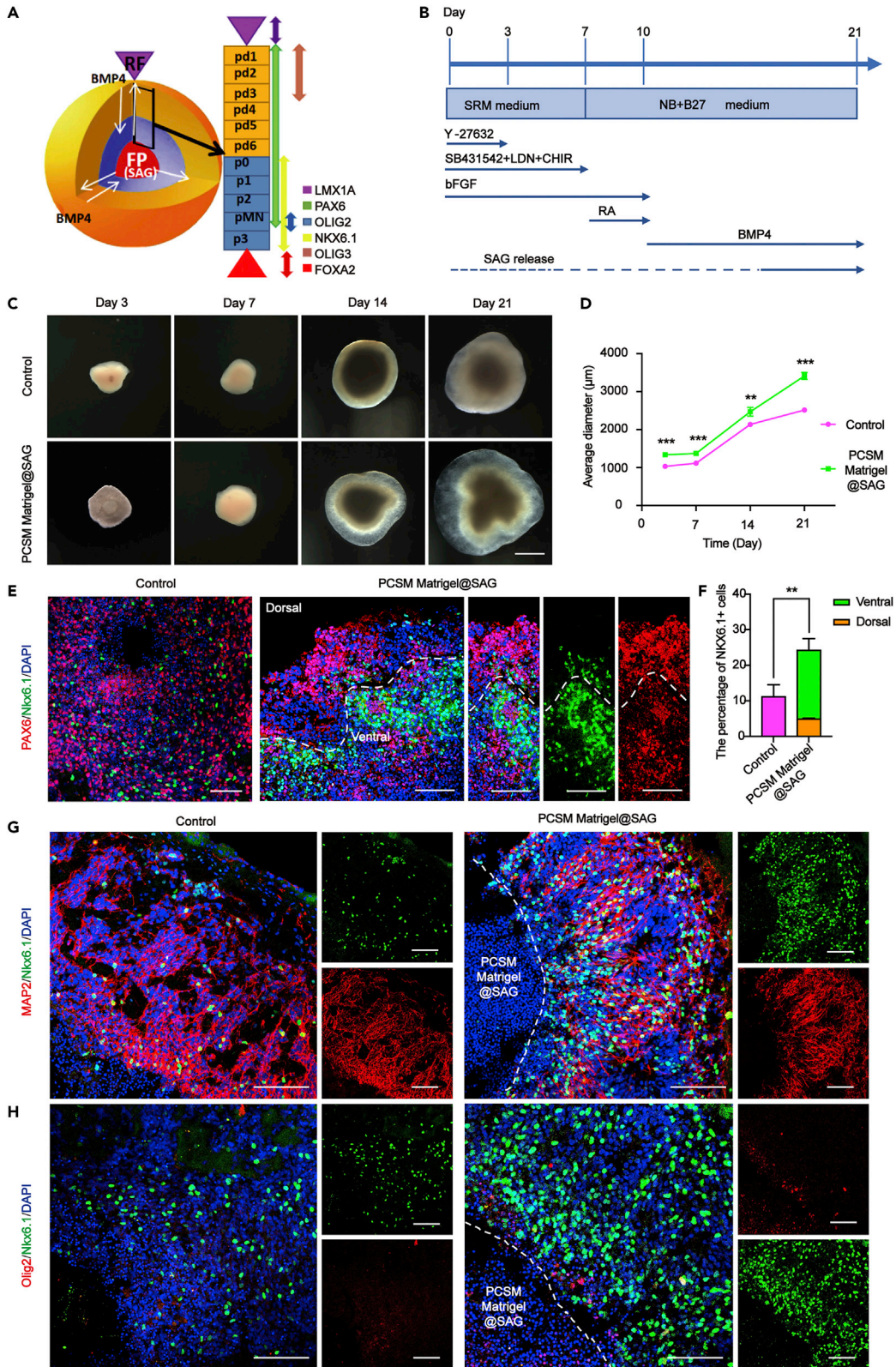


**Figure 2. Identification of spinal cord domain progenitor cells in ehSC-organoids**

- (A) The schema of domain-specific distribution and representative markers of neural progenitor cells in developmental spinal cord.  
(B) A schematic diagram of the induction of ehSC-organoids.  
(C) Representative phase images of the control organoids and ehSC-organoids from day 3 to day 21. Scale bars, 1 mm.  
(D) A statistical chart of the diameter dynamic change of ehSC-organoids.  
(E) Expression patterns of spinal cord domain progenitor markers of the control organoids and ehSC-organoids. Scale bars, 100  $\mu$ m.  
(F) The percentage of ventral Nkx6.1+ cells in spinal cord organoids.  
(G) Expression patterns of the spinal cord ventral progenitor and neuronal marker in the control organoids and ehSC-organoids. Scale bars, 100  $\mu$ m.  
(H) Expression patterns of spinal cord ventral progenitor markers of the control organoids and ehSC-organoids. Control organoids: without PCSM-Matrigel@SAG; ehSC-organoids: with PCSM-Matrigel@SAG.

Olig2+ progenitor cells were also observed close to PCSM-Matrigel@SAG and some coexpressed NKX6.1 (Figure 2H), suggesting that the PCSM-Matrigel@SAG organizer controlled the spinal cord organoids with ventral domain progenitor cell identities through the release of SAG. Correspondingly, dorsal Olig3+ spinal cord progenitors, which could be controlled by outside BMP4 signaling, were mainly distributed in the outer layer of ehSC-organoids (Figures S2C, S2D). Spinal cord PAX6+ progenitor cells presented in both ventral and dorsal progenitor domains, while ventral Olig2+ and NKX6.1+ cells were hardly observed in dorsal domains (Figures 2E, 2G, 2H, and S2D). However, more Olig3+ dorsal progenitor cells localized in the outside layer of organoids that were not induced using PCSM-Matrigel@SAG (Figures S2C, S2D), which confirms that ventral signaling SAG is vital for the generation of ventral progenitor cells. Besides, we also detected the expression of GFAP and MBP to evaluate the glial cells. The results showed that D21-organoids displayed no difference in the population of glia cells (Figures S2E-S2G). Taken together, PCSM-Matrigel@SAG scaffolds can mimic the ventral spinal cord organizing center, allowing the induction of ventral domain progenitor cells in ehSC-organoids.

**Identification of spinal cord neurons in ehSC-organoids**

To generate domain-specific spinal cord subtype neurons, ehSC-organoids were further cultured to day 42, and immunostaining was performed to identify spinal cord motor neurons (Figure 3A). We found that the majority of ChAT+/MAP2+ neurons adjacent to the PCSM-Matrigel@SAG scaffold formed ventral horn-like clusters in 42-day-old ehSC-organoids. However, the organoids without the PCSM-Matrigel@SAG scaffold demonstrated no spatial dorsal-ventral distribution of ChAT+/MAP2+ neurons (Figures 3B and 3C). The percentage of ChAT+ neurons in ehSC-organoids was higher than that in control organoids (Figure 3D). The spinal cord motor neuron marker HB9 was more highly expressed in ehSC-organoids than in the control group and coexpressed with MAP2, indicating their identity as ventral spinal cord motor neurons (Figures 3E and 3F). We further detected interneurons in the ventral horn of the spinal cord. Immunostaining showed that Lhx1 and Lhx3 expression was not observed in the control group. However, we found regional distribution of Lhx1+ and Lhx3+ cells in the PCSM-Matrigel@SAG-induced organoids (Figures 3G-3I). These results indicated that V0, V1, and V2a neurons were successfully induced in ehSC-organoids. In addition, a large number of GAD67+ inhibitory neurons and VGlut1+ excitatory neurons were detected in 6-week-old ehSC-organoids (Figures S3A and S3B). However, less dorsal and ventral neurons of different subtypes were observed in spinal cord organoids without PCSM-Matrigel@SAG treatment and with no significant dorsal-ventral spatial distribution (Figures 3C, 3E and S3A, S3B). We also found D42-organoids displayed GFAP and MBP expression differences in the both groups. GFAP expression was higher in the control group than that in the PCSM Matrigel@SAG group while MBP showed an opposite trend (Figures S3C-S3E). The higher MBP expression may contribute to the maturation of neurons in the PCSM Matrigel@SAG group. In summary, these results demonstrated that the PCSM-Matrigel@SAG organizer successfully induced ventral spinal cord motor neurons, including major subtypes of neurons in the ehSC-organoids.

**Induction of the ehSC-organoids from induced pluripotent stem cells**

Human induced pluripotent stem cells (hiPSCs) derived from patients' somatic cells with the same genetic background could be widely used for modeling the pathogenesis of neural diseases. To develop personalized ehSC-organoids models from hiPSCs, we performed human fibroblast cell reprogramming using nonviral and integration-free episomal vectors, which may facilitate clinical applications of the ehSC-organoids in the future.<sup>21</sup> After plasmid electroporation, human fibroblast cells were reprogrammed into hESC-like colonies at day 25 (Figures S4A and S4B). We picked single colonies and expanded them in an E8 medium (Figure S4C). Through immunofluorescence staining, pluripotent stem cell markers such as OCT4, SOX2, SSEA4, and TRA-1-60 were all shown to be highly expressed in these colonies (Figure S4D),

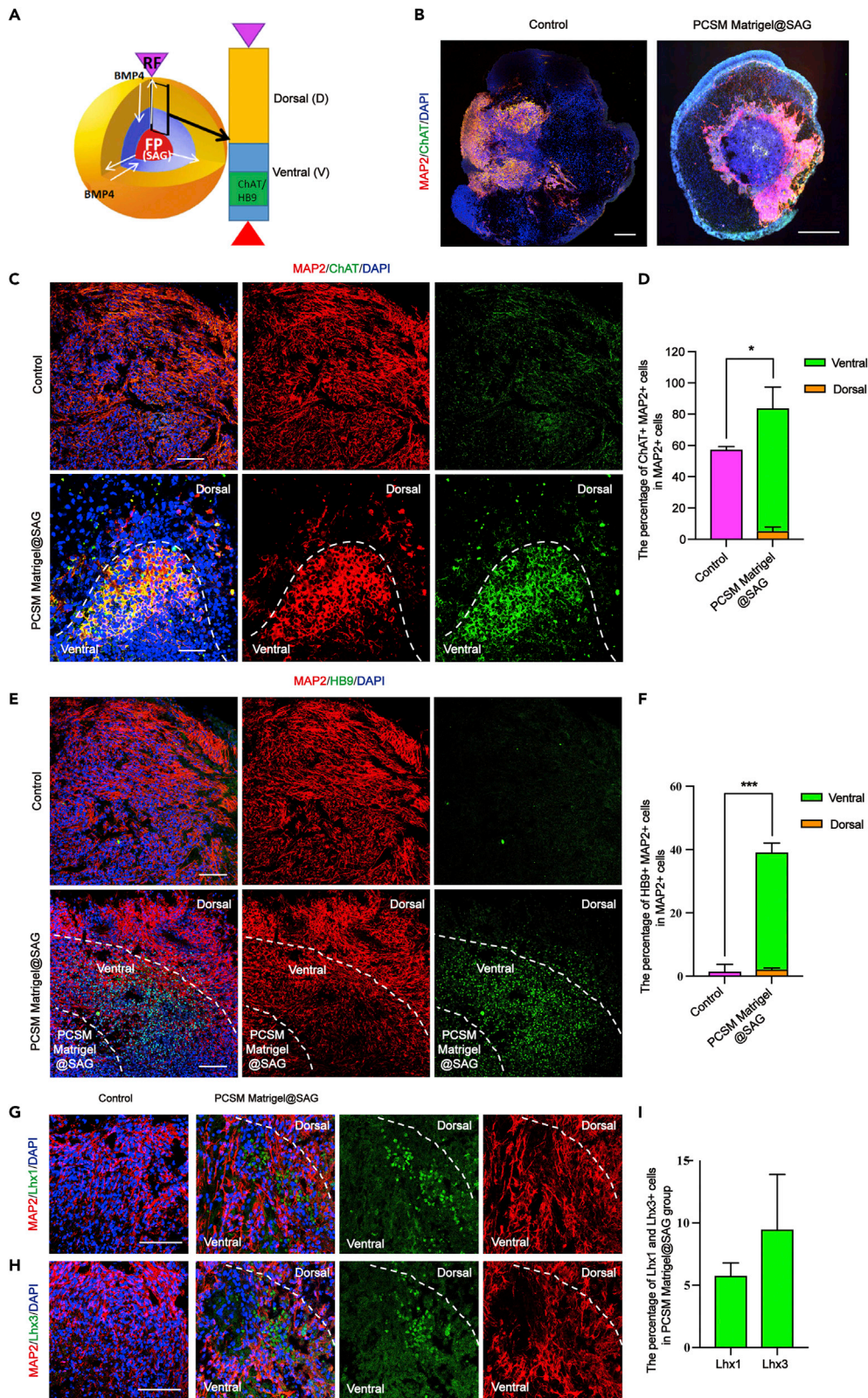


**Figure 3. Identifying spinal cord subtype neurons of the ehSC-organoids**

(A) Motor neuron distribution in the ehSC-organoids.

(B) Spatial patterns of MAP2 and ChAT positive neurons of ehSC-organoids at week 6. Scale bars: 200  $\mu\text{m}$  (left) and 500  $\mu\text{m}$  (right).

(C and E) Representative images of coexpression of MAP2+/ChAT+ and MAP2+/HB9+ neurons in the control organoids and ehSC-organoids at week 6. Scale bars: 50  $\mu\text{m}$  (C) and 100  $\mu\text{m}$  (E).

(D and F) The percentage of MAP2+/ChAT+ and MAP2+/HB9+ neurons in spinal cord organoids induced through different methods.

(G and H) Representative images of Lhx1+ or Lhx3+ neurons in the control organoids and ehSC-organoids at week 6. Scale bars, 100  $\mu\text{m}$ .

(I) The percentage of Lhx1+ and Lhx3+ neurons in spinal cord organoids induced through PCSM-Matrigel@SAG. Control organoids: without PCSM-Matrigel@SAG; ehSC-organoids: with PCSM-Matrigel@SAG.

demonstrating their pluripotent stem cell identities. Using the PCSM-Matrigel@SAG scaffold, we reconstructed spinal cord organoids using hiPSCs. Similar to hESCs, hiPSCs were well integrated with PCSM-Matrigel@SAG and grew well to form ehSC-organoids (Figure 4A). Subsequently, we performed immunostaining for the identification of hiPS-ehSC-organoids at 21 and 42 days. We found that ventral NKX6.1+ progenitor cells were aggregated outside the PCSM-Matrigel@SAG scaffold (Figures 4B and 4C). We also observed that Olig2+ motor neuron progenitor cells were colocalized and clustered with NKX6.1+ cells (Figure 4C). Similarly, Olig3+ cells were mainly located at the outside layer of hiPS-ehSC-organoids (Figure 4D). In 42-day-old hiPS-ehSC-organoids, we found that most ChAT+/MAP2+ neurons were adjacent to the PCSM-Matrigel@SAG scaffold, forming the ventral horn-like clusters (Figure 4E). The motor-neuron-specific marker gene *HB9* was also coexpressed with MAP2+ neurons, indicating their ventral spinal cord motor neuronal identity (Figure 4F). Furthermore, both GAD67+ inhibitory and VGlut1+ excitatory neurons were detected in 6-week-old iPS-ehSC-organoids (Figures 4G and 4H). In conclusion, the induction method of ehSC-organoids showed consistent results in human pluripotent stem cells.

**Single-cell RNA-sequencing analysis of the ehSC-organoids**

To further investigate the identity of ehSC-organoids cells, we performed single-cell RNA sequencing. Gene expression profiles of 15,813 cells from three 6-week-old ehSC-organoids were generated using the 10x Genomics platform. After quality control, 11,433 cells, which expressed between 1,000 and 6,000 genes, were used for further analysis. Gene expression of each cell was normalized and scaled using the R package Seurat. Cells were clustered based on the principal component analysis and construction of a nearest-neighbor graph. We found that cells grouped into 16 main clusters and then labeled these clusters as spinal cord domain-specific cell types according to the expression of known markers.<sup>22</sup> Specifically, ehSC-organoids at 6 weeks contained two main subtypes of cells: neural progenitors and neurons. The neural progenitors represented about 31% of the total number of cells and could be subdivided into RP, dp1-6, p0/1/2, and pMN/p3/FP cell clusters, while the neuronal cells contained dl1-3, dl4-6, v0, v1, v2, and MN spinal cord regional clusters (Figure 5A). Neuronal clusters of dl4-6 compose the largest proportion (36.4%), followed by neural progenitors of p0/1/2 (24.5%) (Figure 5A). In addition, multiple known neural marker genes, such as *SOX2*, *MAP2*, *TUBB3*, and *PAX6*, showed high expression in 6-week-old ehSC-organoids (Figure 5B). Bubble charts revealed the expression patterns of spinal cord dorsal and ventral region-specific markers in each assigned cell cluster, demonstrating their developmental spinal cord identities (Figure 5C). Furthermore, we found GABAergic neurons (GAD1+, SLC32A1+, and GAD2+) were broadly expressed in multiple cell clusters, while glutamatergic (SLC17A6+), glycinergic (SLC6A5+), and cholinergic (SLC5A7+ and SLC18A3+) cells were mainly expressed in domains dl1-6 and v1 (Figure 5D). We found the extensive expression of *HOXA2*-*HOXA6*, *HOXB2*-*HOXB9*, *HOXC4*-*HOXC9*, *HOXD3*, *HOXD4*, and *HOXD8* in ehSC-organoids, indicating their caudal cervical/thoracic spinal cord identities (Figure 5E). To confirm the single-cell RNA-sequencing results, we measured the expression of HOX proteins. The results showed both *Hoxc9* and *Hox10* were expressed in 42-day-old ehSC-organoids, reaching 39.90% and 7.51%, respectively (Figures 5F–5H), which demonstrated the caudal characteristic of human spinal cord cells in ehSC-organoids. In summary, these results verified that these ehSC-organoids possess the developmental spinal cord identities, with dorsa-ventral and rostro-caudal spatial cytoarchitecture.

**Functional connectivity in ehSC-organoids**

To characterize the neuronal function of ehSC-organoids, we next detected intracellular calcium activity in spinal cord organoids by labeling calcium with Oregon Green 488 BAPTA-1 indicator and using two-photon calcium imaging. We found that calcium activity could be detected in the ehSC-organoids at

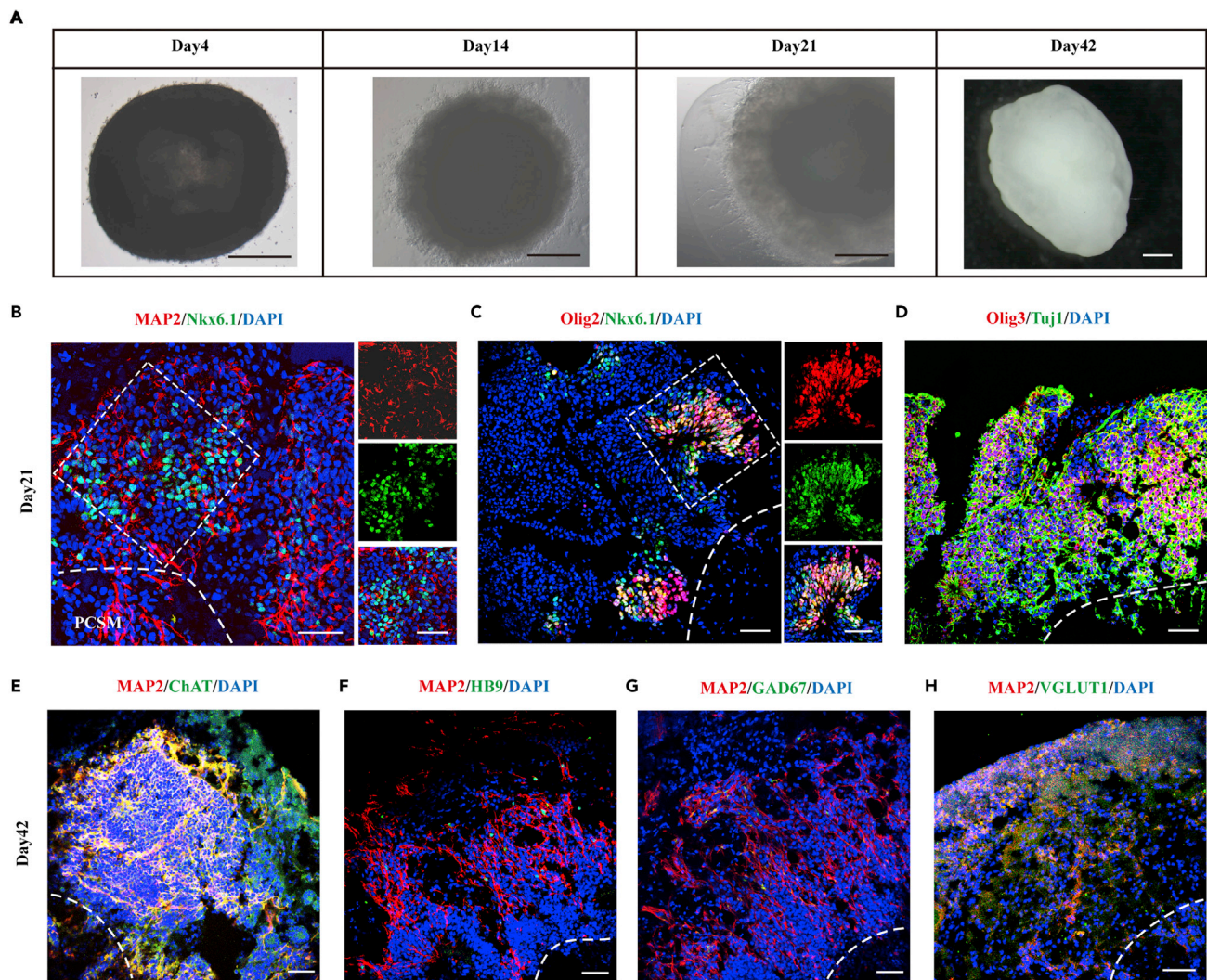


**Figure 4. The induction of iPSC-ehSC-organoids with PCSM-Matrigel@SAG**

(A) Representative phase images of iPSC-ehSC-organoids at different stages. Scale bars, 500  $\mu\text{m}$ .

(B-D) Expression patterns of dorsoventral spinal cord progenitor markers of iPSC-ehSC-organoids at week 3 by NKX6.1, Olig2, and Olig3. Scale bars, 50  $\mu\text{m}$ .

(E-H) Expression patterns of spinal cord neuronal markers of iPSC-ehSC-organoids at week 6 by MAP2, ChAT, HB9, GAD67, and VGLut1. Scale bars, 50  $\mu\text{m}$ . ehSC-organoids: with PCSM-Matrigel@SAG.

week 8 (Figures 6A and 6B). Of the total 200 neurons, 66.8% in ehSC-organoids responded with enhanced calcium spikes following a stimulus with KCl, which suggested that there were many functionally active neurons in the 8-week-old ehSC-organoids (Figures 6B and 6C). These results demonstrated spontaneous individual neuronal activity in the ehSC-organoids. To evaluate the whole neural network activity in 3D ehSC-organoids, we adopted calcium time-lapse imaging to detect calcium signal dynamics in the intact ehSC-organoids. We divided the whole field of imaging of the ehSC-organoids into regions of interest ( $\sim 450 \mu\text{m} \times 450 \mu\text{m}$ ) and measured the calcium network activity. We found that high-KCl treatment induced bursting calcium activities, which could be blocked by NBQX, a highly selective and competitive AMPA receptor antagonist (Figures 6D and 6E). This demonstrated that the ehSC-organoids possess neural network activity. In summary, these findings demonstrated that our induced ehSC-organoids established neuronal functions with neural network activity.

### A 3D ehSC-organoids model for drug testing

Compared with 2D cultured neural cells, 3D brain organoids derived from hPSCs could replicate the human brain's cytoarchitecture and provide new insights into disease pathogenesis in the human brain.<sup>3,12</sup>

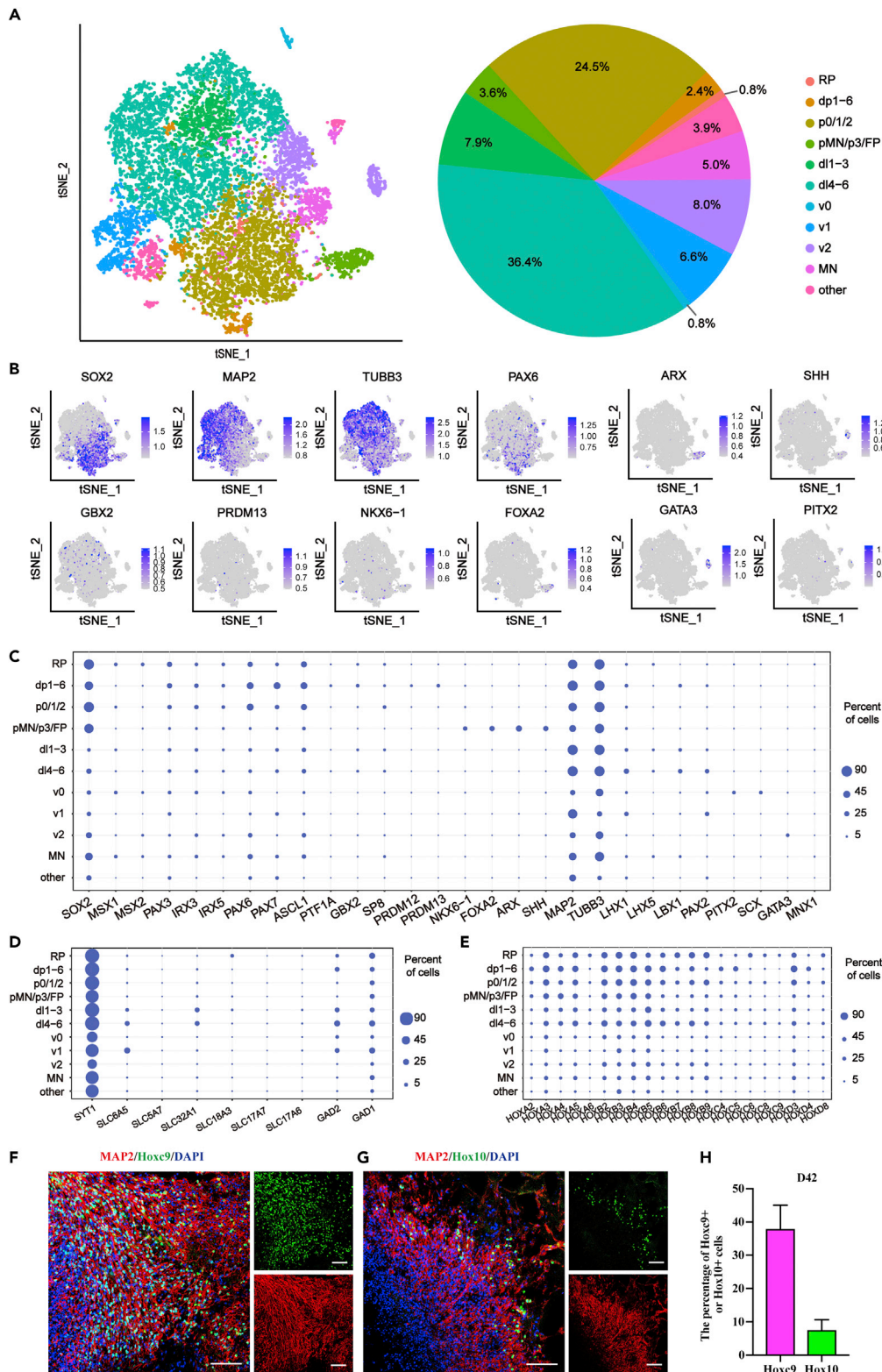


**Figure 5. Single-cell RNA sequencing of ehSC-organoids**

(A) tSNE Plot of single-cell expression of 6-week-old ehSC-organoids ( $n = 11,433$  cells). tSNE: t-distributed Stochastic Neighbor Embedding.

**Figure 5. Continued**

(B) tSNE Plots showing gene expression of cluster-specific markers.

(C-E) Dot plots showing the expression of selected cluster-specific genes, neurotransmitter identity-related genes, and HOX genes of each cluster in ehSC-organoids.

(F) Representative images of Hoxc9+ and MAP2+ cells in the D42-ehSC-organoids. Scale bars, 100  $\mu$ m.

(G) Representative images of Hox10+ and MAP2+ cells in the D42-ehSC-organoids. Scale bars, 100  $\mu$ m.

(H) The percentage of Hoxc9+ and Hox10+ cells in spinal cord organoids induced through PCSM-Matrigel@SAG. ehSC-organoids: with PCSM-Matrigel@SAG.

ehSC-Organoids may have great potential in drug testing for spinal cord diseases. Edaravone, as a potent free radical scavenger, was found to be effective in slowing amyotrophic lateral sclerosis (ALS) progression during early stages of the disease.<sup>23,24</sup> The exact cellular and molecular mechanism of edaravone in slowing ALS is uncertain. To confirm the functionality of edaravone in human spinal cord tissue, we used the ehSC-organoids as a 3D model to test the effects of edaravone. Oxidative stress, which is considered to be the main contributing factor of the pathogenesis of ALS, was mimicked by hydrogen peroxide treatment in 8-week-old ehSC-organoids. After hydrogen peroxide treatment, ehSC-organoids were then treated with edaravone for 3 days and then sliced for immunostaining with neural markers MAP2 and NeuN and the early cell apoptosis marker caspase3. The ehSC-organoids treated with hydrogen peroxide displayed many apoptotic cells. After treatment with edaravone, the number of total apoptotic cells and apoptotic neurons (MAP2+ and NeuN+) significantly reduced (Figures 7A–7D). Taken together, these results suggest that the ehSC-organoid is an efficient 3D model for testing drugs targeted for motor neuron diseases.

## DISCUSSION

Precise organ regeneration or reconstruction *in vitro* or *in vivo* is still challenging, especially central nervous system (CNS) organs, as human brain is the most complex tissue of the human body, with fine spatial and temporal cytoarchitecture.<sup>3,25–28</sup> Here, to rebuild spinal cord organoids *in vitro* with *in vivo*-like cellular topography, we developed a novel method to generate 3D ehSC-organoids via PCSM-Matrigel@SAG. These ehSC-organoids possess most of the ventral and dorsal spinal cord progenitor domains and subtype neurons, show functional neural activity, and can mimic MNDs. These bioengineered ehSC-organoids will hold great potential for modeling spinal cord diseases, drug testing, and SCI regeneration.

The gradients of morphogens, such as Shh, BMP4, and WNTs, control the topography of specific regions of the human brain.<sup>10,15,27,29–31</sup> Recently, 1 study has reported that a WNT-activating gradient in a microfluidic device mimicked the rostral-caudal neural axis specification in an early developing stage of the human neural tube.<sup>31</sup> In addition, the dose gradient of Shh would specify the positional identity of human forebrain organoids by a distance-dependent manner.<sup>30</sup> Here, our study showed that PCSM-Matrigel@SAG as an organizing center could release SAG to ventralize spinal cord organoids *in vitro*. Compared with engineered cell lines with inducible Shh expression, PCSM-Matrigel@SAG scaffolds are much more reproducible and easier to control by changing the compound concentration and could be loaded with different kinds of inducing factors. Thus, they hold more potential for the specification of positional identities of brain-region-specific organoids. Furthermore, biodegradable PCSMs showed low toxicity, which may facilitate their use in tissue engineering and organ regeneration.<sup>32–41</sup> However, the layered architecture of these organoids showed regional heterogeneity, so they do not fully mimic the *in vivo* cellular topography of the human spinal cord. One of the main reasons is the difficulty in self-organization of PCSM-Matrigel@SAG microspheres in the center of the hPSCs at the initial stage, which may lead to the heterogeneous concentration gradient of SAG from the center to the outside. A further reason may be the heterogeneous responses of hPSCs to inducing neural morphogens such as Shh and BMP4, which may influence the regional heterogeneity in cell proliferation and growth and finally lead to heterogeneous neural cell populations and maturation.

In recent years, 3D organoids have become integral tools in tissue and disease modeling.<sup>3,25,27</sup> The development of 3D spinal cord organoids from human pluripotent stem cells has been reported.<sup>13–15,42</sup> However, these studies did not develop spinal cord organoids with *in vivo*-like topography because of the difficulty in constructing two organizing centers of developmental spinal cord *in vitro*. In this study, to mimic these two *in vivo* organizing centers, we constructed a PCSM-Matrigel@SAG scaffold to function as a SAG-released organizing center and controlled outside treatment of BMP4 as a dorsal signaling organizer using these tools. We successfully generated 3D dorsoventralizing spinal cord organoids. There is some central necrosis in ehSC-organoids without vascularization or sufficient oxygen penetration, which

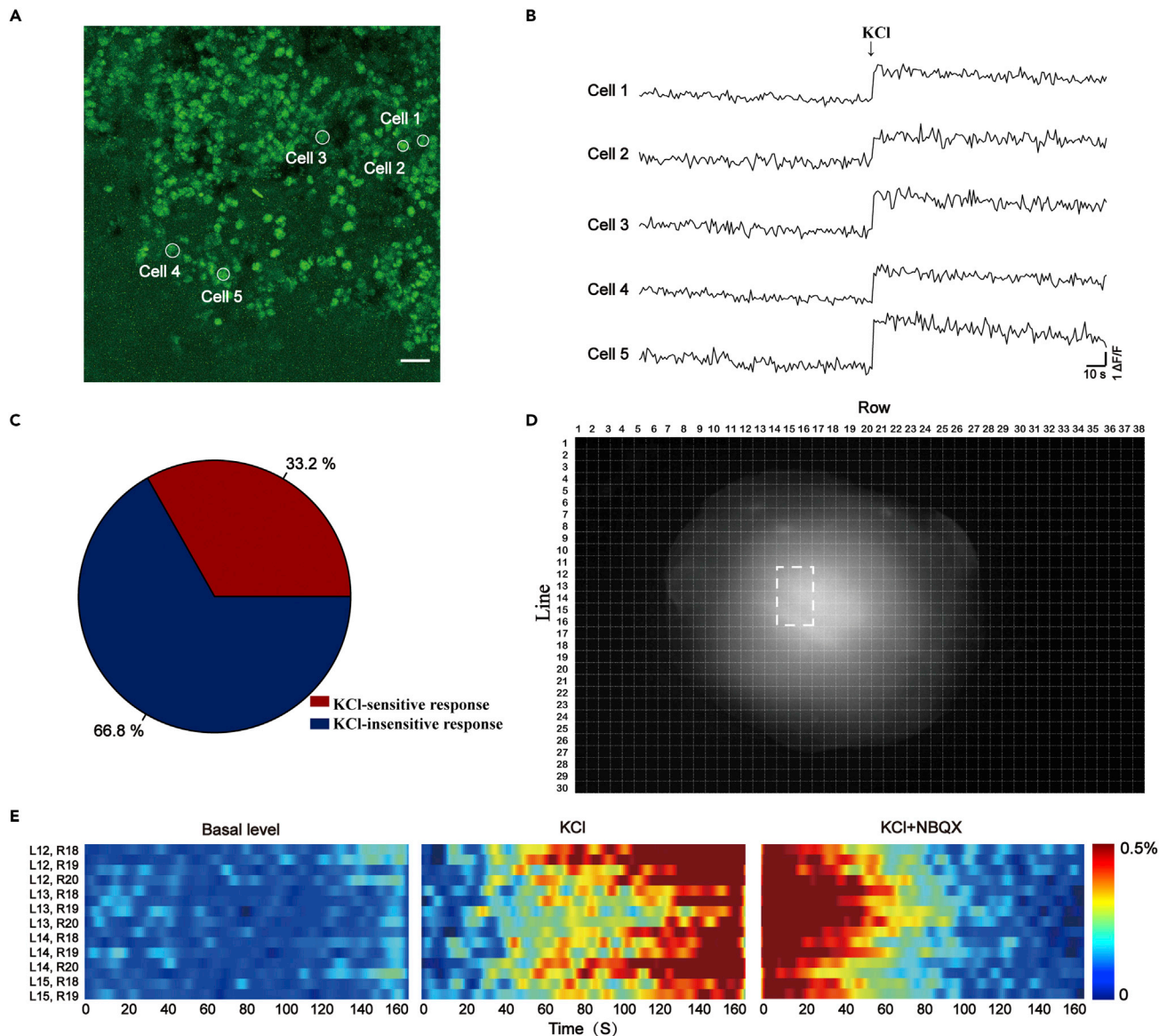


**Figure 6. Functional calcium activity in ehSC-organoids**

(A) Calcium imaging of 8-week-old ehSC-organoids using Oregon Green 488 BAPTA-1. Scale bars, 20  $\mu$ m.

(B) Representative  $\Delta F/F$  traces before and after KCl treatment.

(C) Population of response cells for KCl.

(D) Whole calcium imaging of the ehSC-organoids.

(E) Calcium dynamic activity in ehSC-organoids at week 8 treated with KCl and NBQX.

may be a limitation of medical applications. We will further optimize the induced method to reduce the necrosis by using a microfluidic chip. In the future, PCSM-Matrigel@SAG scaffolds could be loaded with different kinds of small molecules or morphogenic factors for inducing brain-region-specific organoids or modeling morphogens to control the human developmental brain.

To demonstrate generation of personalized MND models, we developed ehSC-organoids from hiPSCs derived from human somatic cells. We also show that the ehSC-organoids combined with different stress cues were efficient models to address the role of environmental factors on spinal cord development and for drug testing. Edaravone, an Food and Drug Administration-approved drug for the therapy of ALS, has been shown to have antioxidative activity.<sup>23,24,43–45</sup> However, the mechanism of therapeutic action of

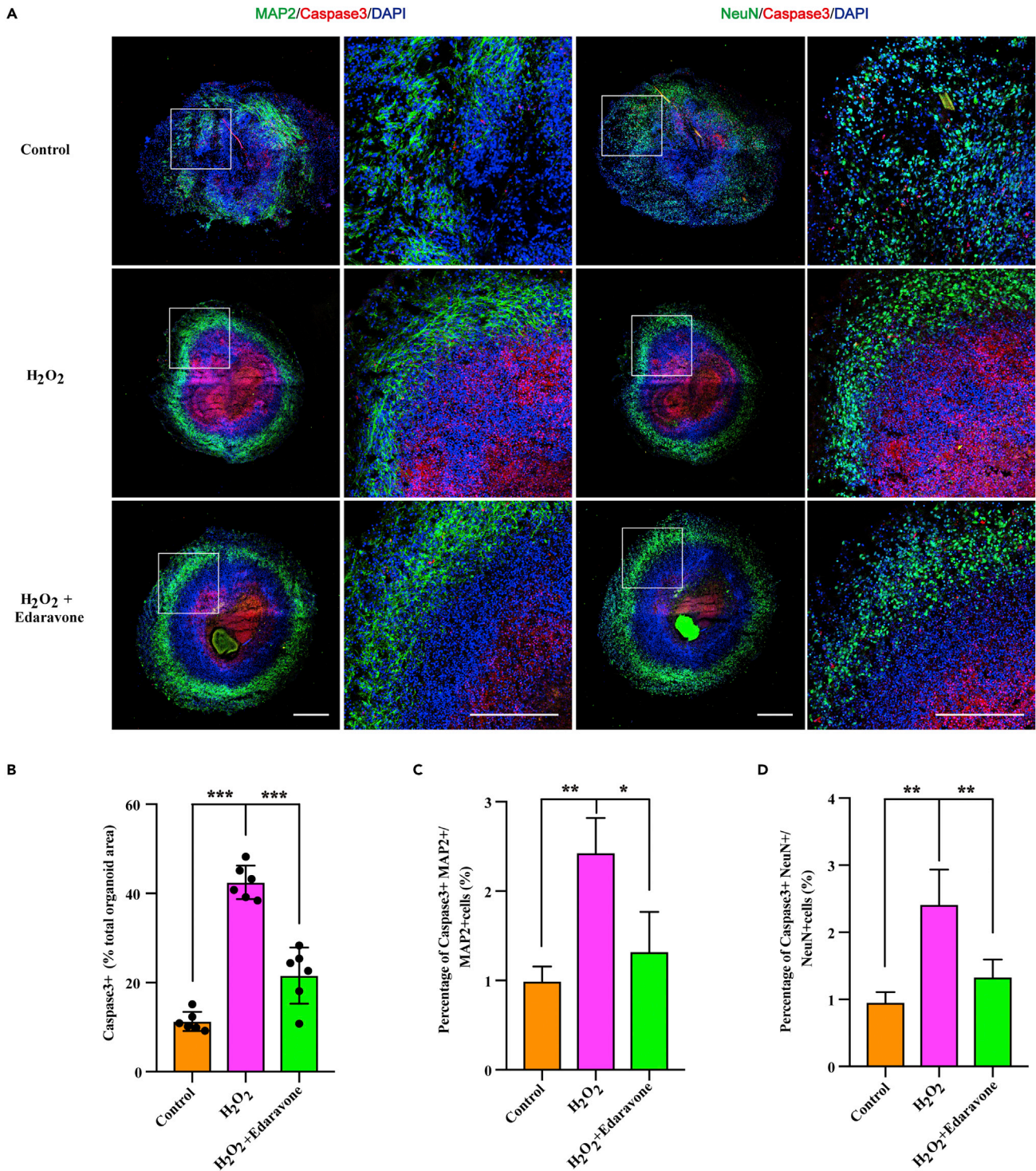


**Figure 7. Testing edaravone in 3D ehSC-organoids**

(A) Immunostaining of ehSC-organoids treated with control, H<sub>2</sub>O<sub>2</sub>, and H<sub>2</sub>O<sub>2</sub> + edaravone at week 8. Scale bars, 250  $\mu$ m.

(B-D) Statistical analysis of the representative images (mean  $\pm$  standard error of mean, n = 6). ehSC-organoids: with PCSM-Matrigel@SAG.

edaravone is still unclear. We tested the effects of edaravone using H<sub>2</sub>O<sub>2</sub>-stressed ehSC-organoids. We found that edaravone may reduce the H<sub>2</sub>O<sub>2</sub>-induced cell apoptosis in ehSC-organoids *in vitro*. In the future, ehSC-organoids may open the possibility of large-scale drug screening for potential MND therapies. Furthermore, our ehSC-organoids derived from individual patient's induced pluripotent stem cells will help to develop precision medicine for MND patients.

In summary, we successfully developed a bioengineering process of ehSC-organoids via functional composite scaffolds to mimic the organizing center of developmental neural tube *in vitro*. Furthermore, these ehSC-organoids showed functional neuronal activity and can be used for modeling spinal cord development and drug screening for MND therapies. Techniques to generate more complex ehSC-organoids, with white matter and axon tracts to support the myelination of neuronal axons or to provide relay and regenerate injury to the corticospinal tract, will be important for further studies. Finally, our improved ehSC-organoids may hold promise for use in tissue regeneration of SCI.

### Limitations of the study

One of the limitations of the study is that quantitative gradient sustained release can be achieved through a SAG-released organizing center. In addition, central necrosis in ehSC-organoids exists due to the loss of vascularization. We will resolve the technical construction bottleneck of spinal cord organoids through microfluidic chips in the future.

### STAR★METHODS

Detailed methods are provided in the online version of this paper and include the following:

- KEY RESOURCES TABLE
- RESOURCE AVAILABILITY
  - Lead contact
  - Materials availability
  - Data and code availability
- EXPERIMENTAL MODEL AND SUBJECT DETAILS
  - Cell lines
- METHOD DETAILS
  - Preparation of porous chitosan microspheres (PCSM) and PCSM-Matrigel@SAG
  - SAG release of PCSM-Matrigel@SAG
  - Human pluripotent stem cells culture
  - Toxicity assay
  - Induction of ehSC-organoids
  - Immunofluorescence staining
  - Single-cell RNA-sequencing
  - Calcium imaging of the ehSC-organoids
  - Drug testing of ehSC-organoids
- QUANTIFICATION AND STATISTICAL ANALYSIS

### SUPPLEMENTAL INFORMATION

Supplemental information can be found online at <https://doi.org/10.1016/j.isci.2022.105898>.

### ACKNOWLEDGMENTS

This work was supported by the National Key Research and Development Program of China (2021ZD0202500), Natural Science Foundation of Shanghai (grant 20ZR1405200 to Z.S.), Shanghai Municipal Science and Technology Major Project (no. 2018SHZDZX01) and ZJLab, National Natural Science Foundation of China (grant 32070956 to Z.S., 82101574 to H. Li), and MOE Frontiers Center for Brain Science fund and starting fund from Fudan Universities.

### AUTHOR CONTRIBUTIONS

Z.S., W.X., B.L., and H.L. designed the experiments. W.X., B.L., and H.L. performed the studies. Z.S., W.X., B.L., H.L., and H.L. wrote the manuscript and contributed to date interpretation. Y.X. and B.L. performed

calcium imaging. Z.S., L.R., and W.X. reviewed data interpretation and manuscript contents. Z.S. supported this study financially.

## DECLARATION OF INTERESTS

The authors declare no competing interests.

Received: September 30, 2022

Revised: December 7, 2022

Accepted: December 22, 2022

Published: January 20, 2023

## REFERENCES

- Abad, M., Hashimoto, H., Zhou, H., Morales, M.G., Chen, B., Bassel-Duby, R., and Olson, E.N. (2017). Notch inhibition enhances cardiac reprogramming by increasing MEF2C transcriptional activity. *Stem Cell Rep.* **8**, 548–560. <https://doi.org/10.1016/j.stemcr.2017.01.025>.
- Alizadeh, A., Dyck, S.M., and Karimi-Abdolrezaee, S. (2019). Traumatic spinal cord injury: an overview of pathophysiology, models and acute injury mechanisms. *Front. Neurol.* **10**, 282. <https://doi.org/10.3389/fneur.2019.00282>.
- Vieira de Sá, R., Cañizares Luna, M., and Pasterkamp, R.J. (2021). Advances in central nervous system organoids: a focus on organoid-based models for motor neuron disease. *Tissue Eng. Part C Methods* **27**, 213–224. <https://doi.org/10.1089/ten.TEC.2020.0337>.
- Lee, J.H., Shin, H., Shaker, M.R., Kim, H.J., Park, S.H., Kim, J.H., Lee, N., Kang, M., Cho, S., Kwak, T.H., et al. (2022). Production of human spinal-cord organoids recapitulating neural-tube morphogenesis. *Nat. Biomed. Eng.* **6**, 435–448. <https://doi.org/10.1038/s41551-022-00868-4>.
- Lu, D.C., Niu, T., and Alaynick, W.A. (2015). Molecular and cellular development of spinal cord locomotor circuitry. *Front. Mol. Neurosci.* **8**, 25. <https://doi.org/10.3389/fnmol.2015.00025>.
- Alaynick, W.A., Jessell, T.M., and Pfaff, S.L. (2011). SnapShot: spinal cord development. *Cell* **146**, 178–178.e1. <https://doi.org/10.1016/j.cell.2011.06.038>.
- Rayon, T., Maizels, R.J., Barrington, C., and Briscoe, J. (2021). Single-cell transcriptome profiling of the human developing spinal cord reveals a conserved genetic programme with human-specific features. *Development* **148**. <https://doi.org/10.1242/dev.199711>.
- Gouti, M., Metzis, V., and Briscoe, J. (2015). The route to spinal cord cell types: a tale of signals and switches. *Trends Genet.* **31**, 282–289. <https://doi.org/10.1016/j.tig.2015.03.001>.
- Chizhikov, V.V., and Millen, K.J. (2004). Mechanisms of roof plate formation in the vertebrate CNS. *Nat. Rev. Neurosci.* **5**, 808–812. <https://doi.org/10.1038/nrn1520>.
- Jessell, T.M. (2000). Neuronal specification in the spinal cord: inductive signals and transcriptional codes. *Nat. Rev. Genet.* **1**, 20–29. <https://doi.org/10.1038/35049541>.
- Kadoshima, T., Sakaguchi, H., Nakano, T., Soen, M., Ando, S., Eiraku, M., and Sasai, Y. (2013). Self-organization of axial polarity, inside-out layer pattern, and species-specific progenitor dynamics in human ES cell-derived neocortex. *Proc. Natl. Acad. Sci. USA* **110**, 20284–20289. <https://doi.org/10.1073/pnas.1315710110>.
- Langhans, S.A. (2018). Three-dimensional in vitro cell culture models in drug discovery and drug repositioning. *Front. Pharmacol.* **9**, 6. <https://doi.org/10.3389/fphar.2018.00006>.
- Ogura, T., Sakaguchi, H., Miyamoto, S., and Takahashi, J. (2018). Three-dimensional induction of dorsal, intermediate and ventral spinal cord tissues from human pluripotent stem cells. *Development* **145**, dev162214. <https://doi.org/10.1242/dev.162214>.
- Faustino Martins, J.M., Fischer, C., Urzi, A., Vidal, R., Kunz, S., Ruffault, P.L., Kabuss, L., Hube, I., Gazzo, E., Birchmeier, C., et al. (2020). Self-organizing 3D human trunk neuromuscular organoids. *Cell Stem Cell* **26**, 172–186.e6. <https://doi.org/10.1016/j.stem.2019.12.007>.
- Andersen, J., Revah, O., Miura, Y., Thom, N., Amin, N.D., Kelley, K.W., Singh, M., Chen, X., Thete, M.V., Walczak, E.M., et al. (2020). Generation of functional human 3D cortico-motor assembloids. *Cell* **183**, 1913–1929.e26. <https://doi.org/10.1016/j.cell.2020.11.017>.
- Miura, Y., Li, M.Y., Birey, F., Ikeda, K., Revah, O., Thete, M.V., Park, J.Y., Puno, A., Lee, S.H., Porteus, M.H., and Paşca, S.P. (2020). Generation of human striatal organoids and cortico-striatal assembloids from human pluripotent stem cells. *Nat. Biotechnol.* **38**, 1421–1430. <https://doi.org/10.1038/s41587-020-00763-w>.
- Xu, J., Fang, S., Deng, S., Li, H., Lin, X., Huang, Y., Chung, S., Shu, Y., and Shao, Z. (2022). Generation of neural organoids for spinal-cord regeneration via the direct reprogramming of human astrocytes. *Nat. Biomed. Eng.* <https://doi.org/10.1038/s41551-022-00963-6>.
- Ali, A., and Ahmed, S. (2018). A review on chitosan and its nanocomposites in drug delivery. *Int. J. Biol. Macromol.* **109**, 273–286. <https://doi.org/10.1016/j.ijbiomac.2017.12.078>.
- Guo, Z., Bo, D., He, Y., Luo, X., and Li, H. (2018). Degradation properties of chitosan microspheres/poly(L-lactic acid) composite in vitro and in vivo. *Carbohydr. Polym.* **193**, 1–8. <https://doi.org/10.1016/j.carbpol.2018.03.067>.
- Wong, C.Y., Al-Salami, H., and Dass, C.R. (2018). Microparticles, microcapsules and microspheres: a review of recent developments and prospects for oral delivery of insulin. *Int. J. Pharm.* **537**, 223–244. <https://doi.org/10.1016/j.ijpharm.2017.12.036>.
- Okita, K., Matsumura, Y., Sato, Y., Okada, A., Morizane, A., Okamoto, S., Hong, H., Nakagawa, M., Tanabe, K., Tezuka, K.I., et al. (2011). A more efficient method to generate integration-free human iPS cells. *Nat. Methods* **8**, 409–412. <https://doi.org/10.1038/nmeth.1591>.
- Delile, J., Rayon, T., Melchionda, M., Edwards, A., Briscoe, J., and Sagner, A. (2019). Single cell transcriptomics reveals spatial and temporal dynamics of gene expression in the developing mouse spinal cord. *Development* **146**, dev173807. <https://doi.org/10.1242/dev.173807>.
- Cho, H., and Shukla, S. (2020). Role of edaravone as a treatment option for patients with amyotrophic lateral sclerosis. *Pharmaceuticals* **14**, 29. <https://doi.org/10.3390/ph14010029>.
- Kuzma-Kozakiewicz, M. (2018). Edaravone in the treatment of amyotrophic lateral sclerosis. *Neurol. Neurochir. Pol.* **52**, 124–128. <https://doi.org/10.1016/j.pjnns.2018.03.004>.
- Dutta, D., Heo, I., and Clevers, H. (2017). Disease modeling in stem cell-derived 3D organoid systems. *Trends Mol. Med.* **23**, 393–410. <https://doi.org/10.1016/j.molmed.2017.02.007>.
- Kumamaru, H., Kadoya, K., Adler, A.F., Takashima, Y., Graham, L., Coppola, G., and Tuszynski, M.H. (2018). Generation and post-injury integration of human spinal cord neural stem cells. *Nat. Methods* **15**, 723–731. <https://doi.org/10.1038/s41592-018-0074-3>.
- Lancaster, M.A., Renner, M., Martin, C.A., Wenzel, D., Bicknell, L.S., Hurles, M.E.,

- Homfray, T., Penninger, J.M., Jackson, A.P., and Knoblich, J.A. (2013). Cerebral organoids model human brain development and microcephaly. *Nature* 501, 373–379. <https://doi.org/10.1038/nature12517>.
28. Sofroniew, M.V. (2018). Dissecting spinal cord regeneration. *Nature* 557, 343–350. <https://doi.org/10.1038/s41586-018-0068-4>.
29. Bagley, J.A., Reumann, D., Bian, S., Lévi-Strauss, J., and Knoblich, J.A. (2017). Fused cerebral organoids model interactions between brain regions. *Nat. Methods* 14, 743–751. <https://doi.org/10.1038/nmeth.4304>.
30. Cederquist, G.Y., Asciola, J.J., Tchiew, J., Walsh, R.M., Cornacchia, D., Resh, M.D., and Studer, L. (2019). Specification of positional identity in forebrain organoids. *Nat. Biotechnol.* 37, 436–444. <https://doi.org/10.1038/s41587-019-0085-3>.
31. Rifes, P., Isaksson, M., Rathore, G.S., Aldrin-Kirk, P., Möller, O.K., Barzaghi, G., Lee, J., Egerod, K.L., Rausch, D.M., Parmar, M., et al. (2020). Modeling neural tube development by differentiation of human embryonic stem cells in a microfluidic WNT gradient. *Nat. Biotechnol.* 38, 1357. <https://doi.org/10.1038/s41587-020-0590-4>.
32. Badhe, R.V., Bijukumar, D., Chejara, D.R., Mabrouk, M., Choonara, Y.E., Kumar, P., du Toit, L.C., Kondiah, P.P.D., and Pillay, V. (2017). A composite chitosan-gelatin bilayered, biomimetic macroporous scaffold for blood vessel tissue engineering. *Carbohydr. Polym.* 157, 1215–1225. <https://doi.org/10.1016/j.carbpol.2016.09.095>.
33. Balagangadharan, K., Dhivya, S., and Selvamurugan, N. (2017). Chitosan based nanofibers in bone tissue engineering. *Int. J. Biol. Macromol.* 104, 1372–1382. <https://doi.org/10.1016/j.ijbiomac.2016.12.046>.
34. Cao, L., Zhang, F., Wang, Q., and Wu, X. (2017). Fabrication of chitosan/graphene oxide polymer nanofiber and its biocompatibility for cartilage tissue engineering. *Mater. Sci. Eng. C Mater. Biol. Appl.* 79, 697–701. <https://doi.org/10.1016/j.msec.2017.05.056>.
35. Aimin, C., Chunlin, H., Juliang, B., Tinyin, Z., and Zhichao, D. (1999). Antibiotic loaded chitosan bar - an in vitro, in vivo study of a possible treatment for osteomyelitis. *Clin. Orthop. Relat. Res.* 239–247. <https://doi.org/10.1097/00003086-199909000-00031>.
36. Dang, J.M., Sun, D.D.N., Shin-Ya, Y., Sieber, A.N., Kostuik, J.P., and Leong, K.W. (2006). Temperature-responsive hydroxybutyl chitosan for the culture of mesenchymal stem cells and intervertebral disk cells. *Biomaterials* 27, 406–418. <https://doi.org/10.1016/j.biomaterials.2005.07.033>.
37. Doench, I., Ahn Tran, T., David, L., Montebault, A., Viguier, E., Gorzelanny, C., Sudre, G., Cachon, T., Louback-Mohamed, M., Horbelt, N., et al. (2019). Cellulose nanofiber-reinforced chitosan hydrogel composites for intervertebral disc tissue repair. *Biomimetics* 4, 19. <https://doi.org/10.3390/biomimetics4010019>.
38. Fiqrianti, I.A., Widiyanti, P., Manaf, M.A., Savira, C.Y., Cahyani, N.R., and Bella, F.R. (2018). Poly-L-lactic acid (PLLA)-Chitosan-Collagen electrospun tube for vascular graft application. *J. Funct. Biomater.* 9, 32. <https://doi.org/10.3390/jfb9020032>.
39. França, D., Medina, Â.F., Messa, L.L., Souza, C.F., and Faez, R. (2018). Chitosan spray-dried microcapsule and microsphere as fertilizer host for swellable - controlled release materials. *Carbohydr. Polym.* 196, 47–55. <https://doi.org/10.1016/j.carbpol.2018.05.014>.
40. Grolík, M., Kuźmicz, D., Dobrowolski, D., Wowra, B., Wylęgała, E., Nowakowska, M., and Szczubiałka, K. (2018). Silicone-modified chitosan membranes for corneal epithelium tissue engineering. *J. Biomater. Tissue Eng.* 8, 374–383. <https://doi.org/10.1166/jbt.2018.1746>.
41. Shamloo, A., Sarmadi, M., Aghababaie, Z., and Vossoughi, M. (2018). Accelerated full-thickness wound healing via sustained bFGF delivery based on a PVA/chitosan/gelatin hydrogel incorporating PCL microspheres. *Int. J. Pharm.* 537, 278–289. <https://doi.org/10.1016/j.ijpharm.2017.12.045>.
42. Duval, N., Vaslin, C., Barata, T.C., Farma, Y., Contremoulins, V., Baudin, X., Nedelec, S., and Ribes, V.C. (2019). BMP4 patterns Smad activity and generates stereotyped cell fate organization in spinal organoids. *Development* 146. <https://doi.org/10.1242/dev.175430>.
43. Ohta, Y., Nomura, E., Shang, J., Feng, T., Huang, Y., Liu, X., Shi, X., Nakano, Y., Hishikawa, N., Sato, K., et al. (2019). Enhanced oxidative stress and the treatment by edaravone in mice model of amyotrophic lateral sclerosis. *J. Neurosci. Res.* 97, 607–619. <https://doi.org/10.1002/jnr.24368>.
44. Sawada, H. (2017). Clinical efficacy of edaravone for the treatment of amyotrophic lateral sclerosis. *Expert Opin. Pharmacother.* 18, 735–738. <https://doi.org/10.1080/14656566.2017.1319937>.
45. Ohta, Y., Yamashita, T., Nomura, E., Hishikawa, N., Ikegami, K., Osakada, Y., Matsumoto, N., Kawahara, Y., Yunoki, T., Takahashi, Y., et al. (2020). Improvement of a decreased anti-oxidative activity by edaravone in amyotrophic lateral sclerosis patients. *J. Neurol. Sci.* 415, 116906. <https://doi.org/10.1016/j.jns.2020.116906>.
46. Osorio, D., and Cai, J.J. (2021). Systematic determination of the mitochondrial proportion in human and mice tissues for single-cell RNA-sequencing data quality control. *Bioinformatics* 37, 963–967. <https://doi.org/10.1093/bioinformatics/btaa751>.

## STAR★METHODS

### KEY RESOURCES TABLE

REAGENT or RESOURCE	SOURCE	IDENTIFIER
<b>Antibodies</b>		
PAX6	Biolegend	Cat# 901301
NKX6.1	Developmental Studies Hybridoma Bank	Cat# F55A12
MAP2	Cell Signaling Technology	Cat# 4542S
Olig2	Millipore	Cat# AB9610
ChAT	Millipore	Cat# AB144P
HB9	Developmental Studies Hybridoma Bank	Cat# 81.5C10-S
Lhx1	Developmental Studies Hybridoma Bank	Cat# 4F2-S
Lhx3	Developmental Studies Hybridoma Bank	Cat# 67.4E12
Olig3	Sigma-Aldrich	Cat# HPA018303
Tuj-1	Biolegend	Cat# 801201
GAD67	Millipore	Cat# MAB5406
VGlut1	UC Davids/NIH NeuroMab	Cat# 75-066
Hoxc9	Abcam	Cat# ab50839
Hox10	Santa Cruz Biotechnology	Cat# SC-365519
Caspase3	Cell Signaling Technology	Cat# 9661S
NeuN	Abcam	Cat# ab104224
GFAP	Abcam	Cat# ab7260
MBP	Biolegend	Cat# 808401
OCT4	BD Biosciences	Cat# 561555
SOX2	Cell Signaling Technology	Cat# 4900S
SSEA4	Millipore	Cat# MAB4304
TRA-1-60	Millipore	Cat# MAB4306
<b>Chemicals, peptides, and recombinant proteins</b>		
Chitosan	Macklin	Cat# C850348
Glacial acetic acid	Macklin	Cat# A801295
S80	Macklin	Cat# S817933
Tween-60	Macklin	Cat# T819614
Dimethyl sulfoxide	Sigma-Aldrich	Cat# D8418
SAG	MedChemExpress	Cat# HY-12848
Matrigel	Corning	Cat# 356230
FGF	PeproTech	Cat# AF-100-18B
TGF- $\beta$	Cell Signaling Technology	Cat# 8915LF
$\beta$ -mercaptoethanol	Sigma-Aldrich	Cat# M3148
LDN193189	MedChemExpress	Cat# HY-12071
SB431542	MedChemExpress	Cat# HY-10431
CHIR99021	Tocris	Cat# 4423
Y27632	MedChemExpress	Cat# HY-10583
B27	ThermoFisher	Cat# 17504044
RA	Sigma-Aldrich	Cat# R2625
BMP4	PeproTech	Cat# 120-05-5
GDNF	PeproTech	Cat# AF-450-10

(Continued on next page)

**Continued**

REAGENT or RESOURCE	SOURCE	IDENTIFIER
BDNF	PeptoTech	Cat# AF-450-02-10
Vitamin C	MedChemExpress	Cat# HY-B0166
Papain enzyme	Worthington	Cat# LS03126
DNase I	Sigma-Aldrich	Cat# 11284932001
Oregon Green™ 488 BAPTA-1	Invitrogen	Cat# O6806
KCl	Innochem	Cat# A44772
NBQX	Macklin	Cat# N873840
H <sub>2</sub> O <sub>2</sub>	Innochem	Cat# A97384
Edaravone	Sigma-Aldrich	Cat# M70800
<b>Critical commercial assays</b>		
Nucleofector kit	Lonza	Cat# VPD-1001
MTT Assay	Abcam	Cat# ab211091
<b>Deposited data</b>		
Single-cell RNA-sequencing data	<a href="https://ngdc.cncb.ac.cn/gsa-human/">https://ngdc.cncb.ac.cn/gsa-human/</a>	Accession: HRA003658
<b>Experimental models: Cell lines</b>		
Human embryonic stem cell line (H9)	Wicell	Agreement No. 22-W0510
Human fibroblasts cell line	ATCC	Cat# CRL-2097
<b>Recombinant DNA</b>		
pCXLE-hOCT3/4-shp53-F	Addgene	Cat# 27077
pCXLE-hSK	Addgene	Cat# 27078
pCXLE-hUL	Addgene	Cat# 27080
<b>Software and algorithms</b>		
Graphpad Prism 8.0	Graphpad software	<a href="https://www.graphpad.com/">https://www.graphpad.com/</a>
ImageJ 2.1.0/1.53c	ImageJ software	<a href="https://imagej.net/Contributors">https://imagej.net/Contributors</a>
MATLAB R2020b	Mathworks	<a href="https://ww2.mathworks.cn">https://ww2.mathworks.cn</a>

**RESOURCE AVAILABILITY****Lead contact**

Further information and requests for resources and reagents should be directed to and will be fulfilled by the Lead Contact, Zhicheng Shao ([zcs hao@fudan.edu.cn](mailto:zcs hao@fudan.edu.cn)).

**Materials availability**

This study did not generate new unique reagents.

**Data and code availability**

All the data reported in this paper will be shared by the [lead contact](#) upon request. This paper does not report original code. Any additional information required to reanalyze the data reported in this paper is available from the [lead contact](#) upon request.

**EXPERIMENTAL MODEL AND SUBJECT DETAILS****Cell lines**

Human fibroblast cells were purchased from ATCC. Cells were expanded in fibroblast medium including DMEM, 10% FBS, 1% GlutaMAX, 1% non-essential amino acids, 10 ng/mL FGF basic, 1% penicillin-streptomycin, 0.1%  $\beta$ -mercaptoethanol. Human embryonic stem cell line (H9) was obtained from Wicell company and cultured in Essential 8 medium. Two cell lines were also cultured in 37°C and 5% CO<sub>2</sub> conditions.

## METHOD DETAILS

### Preparation of porous chitosan microspheres (PCSM) and PCSM-Matrigel@SAG

Porous chitosan microspheres (PCSM) were prepared by micro-emulsification and low temperature thermally induced phase separation (L-TIPS) techniques. First, 10 mg/mL chitosan solution was prepared by dissolving chitosan powder in 1% glacial acetic acid, which was used as the dispersed phase. Solution containing S80, T60 and petroleum ether in a mass ratio (S80/T60/petroleum) of 9.6/0.4/90 served as the continuous phase. Second, 10 mL dispersed phase was slowly added into the continuous phase (50 mL) under stirring at 700 rpm at 40°C, following by continually stirring for 3 h (h) to form a w/o emulsion. After being quenched, emulsion was stored at -20°C for 3–3.5 h, and then was gently dispersed by stirring at 200 rpm for 2 min. Subsequently, 100 mL NaOH solution (10 mg/mL) in volume ratio (ethanol/water) of 14:1 was poured into the emulsion while stirring at 200 rpm to obtain porous chitosan microspheres (PCSM). The PCSM were sequentially processed with 75% ethanol, PBS solution and UV irradiation for sterilization. Approximately 30–40 PCSM and 10  $\mu$ L small molecule SAG (0.5 mM) (HY-12848, MCE) were gently mixed on ice and stored at 4°C for 12 h. Then, 40  $\mu$ L Matrigel (356230, Corning) added and gently mixed on ice before storing at 37°C for 30 min to obtain PCSM-Matrigel@SAG. We used spinal cord organoids grown without PCSM-Matrigel@SAG treatment as a control group.

### SAG release of PCSM-Matrigel@SAG

To confirm the sustained-release function of PCSM-Matrigel@SAG, 20 PCSM-Matrigel@SAG scaffolds were dispersed in 2 mL PBS solution at 37°C to mimic cell culture conditions, including temperature and humidity. From day 0, we collected 200  $\mu$ L reaction solution and added fresh 200  $\mu$ L PBS every other day. The concentration of SAG was calculated by UV absorption spectrum by UV spectrophotometer (UV-3600 plus, Japan). Standard release curve of SAG was referenced to analyze the sustained-release dosage of PCSM-Matrigel@SAG.

### Human pluripotent stem cells culture

hiPSCs were derived from human fibroblast cells by integration-free reprogramming technology using the Nucleofector kit (VPD-1001, Lonza), as per manufacturer's instructions, and the U-020 system.<sup>21</sup> Briefly, Human fibroblast cells were cultured and expanded in fibroblast medium including DMEM (C11995500BT, ThermoFisher), 10% FBS (NATOCOR), 1% GlutaMAX (35050061, ThermoFisher), 1% non-essential amino acids (11140050, ThermoFisher), 10 ng/mL FGF basic (AF-100-18B, PeproTech), 1% penicillin-streptomycin (15140122, ThermoFisher), 0.1%  $\beta$ -mercaptoethanol (M3148, sigma). Then 4.5  $\mu$ g mixture of episomal plasmids, containing pCXLE-hOCT3/4-shp53-F (27077, Addgene), pCXLE-hSK (27078, Addgene) and pCXLE-hUL (27080, Addgene) at a ratio of 1:1:1, was electroporated into  $1-2 \times 10^6$  fibroblast cells to induce iPSCs. Transfected cells were first seeded in 35-mm dish coated with Matrigel and cultured with fibroblast medium for 2 days. After one day, cells were digested and re-seeded in 6-well plates with cell density of  $1-2 \times 10^5$  cells/well. Cells were cultured in E8 medium containing DMEM/F12 (11330032, ThermoFisher) including 13.6  $\mu$ g/mL sodium selenium (S5105, Sigma), 1 mg/mL sodium chloride (S8776, Sigma), 64  $\mu$ g/mL L-Ascorbic acid 2-phosphate (A8960, Sigma), 20  $\mu$ g/mL recombinant human insulin (I2643, Sigma), 10  $\mu$ g/mL human holo-transferrin (T0665, Sigma), 1% penicillin-streptomycin (15140122, ThermoFisher) and 100 ng/mL bFGF, 1.74 ng/mL TGF- $\beta$  (8915LF, CST) for 21 days. After 21 days, hiPSCs colonies were picked to generate stable iPSC lines. Human embryonic stem cells (WA09, WiCell) and hiPSCs were cultured in 60 mm dishes coated with Matrigel in Essential 8 medium for inducing spinal cord organoids.

### Toxicity assay

The toxicity of PCSM to human embryonic stem cells was measured by MTT assay. Briefly, cells were seeded in 96-well plates at  $4 \times 10^3$  cells/well. Then, PCSM was added into each well at a quantity of 0, 1, 5, 10, 15, 20, 25, 30, 35 or 40. After 24 h, PCSMs were washed out using PBS. Next 100  $\mu$ L MTT solution (1 mg/mL) was added, cultures and shaken at 37°C for 4 h. The absorption value at 490 nm was measured by microplate reader (200 PROM Nano, TRCAN). Cell viability was calculated as follows: the relative viability =  $A/A_0 \times 100\%$  (A represents the absorption value of the experimental group,  $A_0$  represents the absorption value of the control group).

### Induction of ehSC-organoids

The induction of ehSC-organoids from hESC cells and hiPSCs was modified according to previous studies.<sup>13</sup> Briefly, hESCs or hiPSCs were added with PCSM-Matrigel@SAG into ultra-low attachment 96-well plates at

$1 \times 10^5$  cells/well, and cultured in SRM medium containing DMEM (C11995500BT, ThermoFisher), 20% knockout serum (A3181502, ThermoFisher), 1% GlutaMAX (35050061, ThermoFisher), and 10  $\mu$ M  $\beta$ -mercaptoethanol (M3148, sigma). From day 0–7, medium was added SRM medium containing 100 nM LDN193189 (HY-12071, MCE), 10  $\mu$ M SB431542 (HY-10431, MCE), 3  $\mu$ M CHIR99021 (4423, Tocris) and 20 ng/mL FGF-basic. 10  $\mu$ M Y27632 (HY-10583, MCE) was added for first 3 days. On day 7, organoids were coated with 15  $\mu$ L Matrigel/organoid and transferred into ultra-low attachment 24-well plates. From day 8–10, Neurobasal medium (21103049, ThermoFisher) with 2% B27 (17504044, ThermoFisher), 20 ng/mL FGF-basic and 100 nM RA (R2625, sigma) was added. From day 11–20, organoids was cultured with Neurobasal medium containing with 15 ng/mL BMP4 (120-05-5, PeproTech). After day 21, the medium was replaced with Neurobasal medium containing with 2% B27, 20 ng/mL GDNF (AF-450-10, PeproTech), 20 ng/mL BDNF (AF-450-02-10, PeproTech) and 200  $\mu$ M Vitamin C.

### Immunofluorescence staining

Organoids were first fixed in 4% paraformaldehyde (PFA) for 30 min at room temperature and washed in PBS solution three times, then soaked in 30% sucrose overnight. Next, organoids were embedded in optimal cutting temperature compound (OCT) and cut into 20  $\mu$ m thick sections. Before immunostaining, dried sections were immersed in boiling citric acid tissue antigen retrieval solution, incubated in 98°C water for 30 min, and then slowly cooled down. Sections were blocked in PBS containing 3% BSA and 0.3% Triton X-100 for 30 min. Organoids sections were then incubated with primary antibodies solution overnight at 4°C. Primary antibodies included MAP2 (rabbit, CST, 4542S, 1:500), Tuj1 (mouse, Biolegend, 801201, 1:500), PAX6 (rabbit, Biolegend, 901301, 1:300), Olig2 (rabbit, Millipore, AB9610, 1:500), NKX6.1 (mouse, DSHB, F55A12, 1:100), Olig3 (rabbit, sigma, HPA018303, 1:50), ChAT (goat, Millipore, AB144P, 1:50), HB9 (mouse, DSHB, 81.5C10-S), GAD67 (mouse, Millipore, MAB5406, 1:500) and VGlut1 (mouse, UC Davids/NIH NeuroMab, 75-066, 1:1000). Subsequently, sections were incubated with secondary antibodies for 1 h then washed with PBS three times at room temperature. Secondary antibodies were M488 (mouse, ThermoFisher, A11001), R594 (rabbit, ThermoFisher, A11012) and G488 (goat, invitrogen, SA5-10086). Finally, sections were sealed with VECTASHIELD (H-1000, VECTOR) for imaging.

### Single-cell RNA-sequencing

The ehSC-organoids were cultured for 6 weeks, then single-cell RNA-seq performed using 10x Genomics. Briefly, three ehSC-organoids were dissociated in single-cell suspension with 10 U/mL papain enzyme (LS03126, Worthington) solution containing 500  $\mu$ g/mL DNase I (11284932001, sigma) at 37°C for 5 min. Then, cells were suspended in Neurobasal medium added with 10% FBS and 10  $\mu$ M Y27632, and were filtered using a 70  $\mu$ m cell strainer. After measuring cell density and viability, final cell density was adjusted to 300–600 cell/ $\mu$ L. Single cell suspension was evenly mixed with enzymes and beads containing barcode information, then wrapped by oil droplets and loaded into the microfluidic “single cross” to form GEMs (Gel Bead-In-EMulsions). Next, cell lysis and reverse transcription reactions were performed in GEMs, and 10x Barcode was connected with the cDNA product. Subsequently, GEMs and the oil droplets were broken, and the cDNA was used as a template for PCR amplification. The quality of amplified products was measured using Agilent 4200 and libraries of single-cell RNA-seq were prepared with the 10x Genomics Chromium Single Cell 3' Library and Gel Bead Kit v3. Finally, sequencing was performed using the Illumina NovaSeq6000 to obtain paired-end 150 bp reads. Reads from 10x Genomics were aligned to the human reference genome (hg38) using Cell Ranger followed by filtering, barcode and UMI counting. Further analysis was performed using R package Seurat after counting reads for each feature in each cell. Cells with between 1000 and 6000 expressed genes detected, as well as under 10% mtDNA content,<sup>46</sup> were used in analysis. Gene expression of cells was normalized and scaled using R package Seurat. The top 1,500 variable genes were selected for principal component analysis (PCA). After nearest-neighbor graph construction (dims = 1:20 in the function FindNeighbors), clusters cells were identified by function FindClusters (resolution = 0.8) in Seurat. Finally, we identified cell clusters according to the expression of known spinal cord markers.<sup>22</sup> The raw sequence data reported in this paper have been deposited in the Genome Sequence Archive (Genomics, Proteomics & Bioinformatics 2021) in National Genomics Data Center (Nucleic Acids Res 2022), China National Center for Bioinformation/Beijing Institute of Genomics, Chinese Academy of Sciences (GSA-Human: HRA003658) that are publicly accessible at <https://ngdc.cnbc.ac.cn/gsa-human>.

### Calcium imaging of the ehSC-organoids

Two-photon imaging was performed using a commercial microscope system (Olympus, FVMPE-RS). Laser (920 nm) average power was in the range of 10–15 mW. This power measurement was made after the

objective (Olympus XLPLN25XWMP2, 25 $\times$ , 1.05 NA). The time-lapse videos were acquired at  $\sim$ 2 Hz (512  $\times$  512 pixels, 2  $\mu$ s per pixel). The field of view was  $\sim$ 254  $\times$  254  $\mu$ m. Before calcium imaging, ehSC-organoids were transferred into 6 cm dishes and incubated for 45 min with Neurobasal medium with 2% B27, 20 ng/mL GDNF, 20 ng/mL BDNF, 200  $\mu$ M Vc and 2  $\mu$ g/mL Oregon Green<sup>TM</sup> 488 BAPTA-1 (O6806, Invitrogen). Medium was replaced with Neurobasal medium supplemented with 2% B27, 20 ng/mL GDNF, 20 ng/mL BDNF and 200  $\mu$ M Vc. Then 120 frames were recorded for basal calcium intensity. Subsequently, 40 mM KCl solution was added into the medium and imaging was also performed for 2 min, 5-min after KCl treatment. ROIs were manually selected and mean fluorescence was calculated for each frame. The density of fluorescence was calculated as follows:  $\Delta F/F = (F - F_0)/F_0$ , in which  $F_0$  was the average mean of fluorescence of all the images.

In addition, calcium waves of ehSC-organoids were recorded using a fluorescent stereoscope (Nikon, M205). Specifically, ehSC-organoids were incubated with 2  $\mu$ g/mL Oregon Green<sup>TM</sup> 488 BAPTA-1 for 45 min, then the fluorescence intensity of the whole ehSC-organoid was recorded for 3 min. After adding 40 mM KCl solution and treating for 5 min, the fluorescence intensity of the ehSC-organoid was recorded by the same parameters. Finally, after 5 min 50  $\mu$ M NBQX treatment, fluorescence intensity was recorded again. Each field of the movie was divided into a 48  $\times$  30 matrices ( $\sim$ 450  $\mu$ m  $\times$  450  $\mu$ m), and the mean fluorescence intensity of each ROI in matrices was calculated for each time frame. Fluorescence intensity was illustrated by MATLAB (Mathworks, R2020b).

### Drug testing of ehSC-organoids

The ehSC-organoids were treated with 20  $\mu$ M H<sub>2</sub>O<sub>2</sub> for 20 min. After washing with culture medium, 400  $\mu$ M Edaravone was added and organoids incubated for 72 h. The control group was cultured without H<sub>2</sub>O<sub>2</sub> and Edaravone. The H<sub>2</sub>O<sub>2</sub> group only treated with 20  $\mu$ M H<sub>2</sub>O<sub>2</sub>. After treatment with Edaravone, ehSC-organoids were cryo-sectioned and underwent immunostaining. Primary antibodies were Tuj1 (mouse, COVANCE, MMS-435P, 1:1000), NeuN (mouse, Abcam, ab104244, 1:500) and Caspase3 (rabbit, CST, 9661S, 1:300).

### QUANTIFICATION AND STATISTICAL ANALYSIS

All statistical analyses were performed using software GraphPad Prism 8.0 (GraphPad Software). Data is shown as mean  $\pm$  SD of three independent experiments. Imaging data analysis was performed using two-tailed t-test for significance. \* $p < 0.05$ , \*\* $p < 0.01$ , \*\*\* $p < 0.001$ .